

# Pareto Self-Supervised Training for Few-Shot Learning

Zhengyu Chen<sup>1,2,3</sup>, Jixie Ge<sup>1,2</sup>, Heshen Zhan<sup>1,2</sup>, Siteng Huang<sup>1,2</sup>, Donglin Wang<sup>1,2\*</sup>

<sup>1</sup> Machine Intelligence Lab (MiLAB), AI Division, School of Engineering, Westlake University

<sup>2</sup> Institute of Advanced Technology, Westlake Institute for Advanced Study

<sup>3</sup> College of Computer Science & Technology, Zhejiang University

{chenzhengyu, gejixie, zhanheshen, huangsiteng, wangdonglin}@westlake.edu.cn

## Abstract

While few-shot learning (FSL) aims for rapid generalization to new concepts with little supervision, self-supervised learning (SSL) constructs supervisory signals directly computed from unlabeled data. Exploiting the complementarity of these two manners, few-shot auxiliary learning has recently drawn much attention to deal with few labeled data. Previous works benefit from sharing inductive bias between the main task (FSL) and auxiliary tasks (SSL), where the shared parameters of tasks are optimized by minimizing a linear combination of task losses. However, it is challenging to select a proper weight to balance tasks and reduce task conflict. To handle the problem as a whole, we propose a novel approach named as Pareto self-supervised training (PSST) for FSL. PSST explicitly decomposes the few-shot auxiliary problem into multiple constrained multi-objective subproblems with different trade-off preferences, and here a preference region in which the main task achieves the best performance is identified. Then, an effective preferred Pareto exploration is proposed to find a set of optimal solutions in such a preference region. Extensive experiments on several public benchmark datasets validate the effectiveness of our approach by achieving state-of-the-art performance.

## 1. Introduction

Although deep learning has achieved great success in a variety of fields, limitations still exist in many practical applications where labeled samples are intrinsically rare or expensive. Different from humans who can easily learn to accomplish new tasks with a few examples, it is difficult for machines to rapidly generalize to new concepts with very little supervision, which draws considerable attention to the challenging *few-shot learning* (FSL) setting. As training large models with few labeled samples leads to overfitting or even non-convergence, conventional deep neural

networks fail to address such a problem.

Recently, *self-supervised learning* (SSL) attracts many researchers for its soaring performance without involving manual labels. By defining pretext tasks to exploit the structural information of data itself, supervisory signals can be easily developed to learn useful general-purpose representations [2, 20, 32]. As self-supervised learning can improve the generalization of the network under the limitation of labeled data, some recent *few-shot auxiliary learning* (FSAL) works [16, 40] take few-shot learning as learning main task with self-supervised auxiliary tasks. To encourage that the few-shot task benefits from auxiliary tasks, some parameters are shared across tasks to inductive knowledge transfer. However, as the objectives of distinct tasks are different and the relationship between objectives is complicated and unknown, optimizing each task not only promotes each other but also naturally conflicts. A typical solution to suppress such conflict is to optimize the shared parameters by minimizing a weighted sum of the empirical risk for each task, where each weight of the empirical risk can be viewed as the trade-off. In previous works [16, 40], these trade-offs are usually set by experience in practical situations. It is difficult to find optimal trade-offs. Moreover, these works [16, 40] attempt to find one single solution for all objectives, which is likely to sacrifice the performance of the main task and be inconsistent with the goal of few-shot auxiliary learning.

According to the above discussion, few-shot auxiliary learning with conflicting objectives requires better modeling of the trade-off between tasks, which is beyond what a linear combination achieves. To overcome the issue, we propose a novel approach named **Pareto self-supervised training (PSST)** for few-shot learning. PSST explicitly casts few-shot auxiliary learning as a multi-objective optimization problem, with the overall objective of finding a Pareto optimal solution of network parameters [27, 28]. However, different from previous works that explore in the global space [28], PSST uses an effective preferred Pareto exploration for FSL. Specifically, PSST decomposes the

\*Corresponding author.

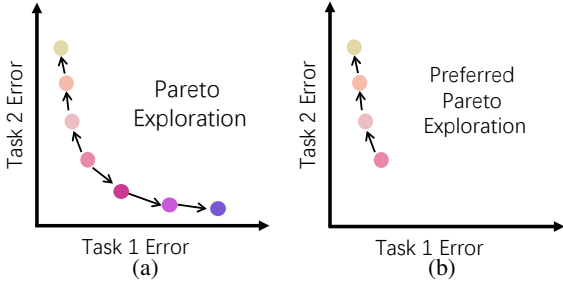


Figure 1: Illustrative examples of Pareto exploration in (a) previous works and (b) our PSST.

few-shot auxiliary problem into several constrained multi-objective subproblems with different trade-off preferences, and then identifies the preference region where the main task achieves the best performance. As illustrated in Fig. 1, the desired space of exploration is thus restricted by only exploring in the preference region where the given points achieve better performance in task 1 rather than task 2. Experiments demonstrate that this improvement can suppress the accumulation of residual error, which contributes to efficiently finding a more accurate Pareto solution. To summarize, our main contributions are as follows:

- We point out that existing few-shot auxiliary learning methods face with a linear combination of conflicting objectives, and propose a multi-objective optimization solution to address the issue.
- We propose a novel Pareto self-supervised training (PSST) approach for few-shot auxiliary learning. To achieve better performance for the main task and meanwhile improve the efficiency and accuracy of the exploration, PSST pioneers a preferred Pareto exploration that explores in the identified preference region.
- We conduct extensive experiments to demonstrate that our PSST can better model the trade-off between tasks, which leads to state-of-the-art performance on several benchmark datasets.

## 2. Related Work

### 2.1. Few-Shot Learning

Few-shot learning aims to generalize well to the novel classes where only a few labeled samples are available. Recently, *meta-learning* has been considered as the main solution to the few-shot problem due to the significant progress. Regarded as “learning to learn”, meta-learning aims to improve its future learning performance with the experience of multiple learning episodes. Current meta-learning approaches for the few-shot problem can be roughly divided into three groups: optimization-based, model-based, and metric-based. *Optimization-based* approaches [5, 6, 13]

learn a meta-learner to adjust the optimization algorithm, usually by providing better initialization or search steps for parameters. *Model-based* [1, 17, 19, 30] approaches depend on well-designed models, whose parameters are obtained with its internal architecture or a meta-learner for fast learning. *Metric-based* approaches [31, 39, 41] learn a generalizable embedding model to transform all samples into a common metric space, where specific distance measures can be employed with the nearest neighbor classifiers.

### 2.2. Self-Supervised Learning

As collecting enough human-annotated labels for large-scale unlabeled data is difficult and expensive, self-supervised learning methods aim to learn representations from unlabeled data. In computer vision applications, various pretext tasks have been utilized for pre-training the network including relative patch location [9], rotation prediction [18], image inpainting [32], and clustering [4]. Another line of works learns representations by contrasting positive pairs against negative pairs constructed on augmented samples [2, 10, 20, 45, 46, 47].

Regarded as auxiliary tasks, self-supervised learning can also be used to improve other tasks. For example, [48] shows that self-supervision can contribute to the recognition in a semi-supervised setting, and [3] uses self-supervision to improve domain generalization. Recently, few-shot auxiliary learning that exploits the complementarity of both few-shot learning and self-supervised learning has drawn much attention. Showing that the auxiliary loss without labels can extract discriminative features for few-shot learning, [16] considers rotation prediction and relative patch location as self-supervised tasks, and [40] uses image jigsaw puzzle. In our work, instead of being limited to specific self-supervised auxiliary tasks, we propose a general and effective preferred Pareto exploration that applies to arbitrary auxiliary tasks.

### 2.3. Multi-Objective Optimization

Multi-objective optimization [51] aims at finding a set of Pareto solutions with different trade-offs rather than one single solution. It has been used in many machine learning applications such as reinforcement learning [43], Bayesian optimization [21] and neural architecture search [12]. As the gradient information is usually not available in these applications, population-based and gradient-free multi-objective evolutionary algorithms [8, 50] are popular methods to find a set of well-distributed Pareto solutions in a single run. However, it can not be used for solving large-scale and gradient-based multi-task learning (MTL) problems. Multi-objective gradient descent [14] is an efficient approach for multi-objective optimization when gradient information is available. [38] proposes a novel method for solving MTL by treating it as multi-objective optimiza-

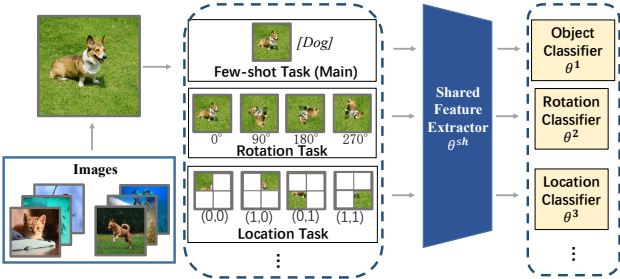


Figure 2: The framework used in our Pareto self-supervised training.

tion. [27] presents an MGDA-based method to generate a discrete set of solutions evenly distributed on the Pareto front. And [28] proposes to replace discrete solutions with continuous solution families, allowing for a much denser set of solutions and continuous analysis on them. However, these methods still focus on how to find a Pareto solution where the performance of each task is equally important. How to effectively find a Pareto solution that is concerned only with the performance of the main task still remains a challenge for auxiliary learning.

### 3. Pareto Self-Supervised Training

In this section, we firstly introduce a general framework to state our problem to be solved. Then we formulate the problem as a multi-objective optimization for FSAL. After that, we elaborate how to solve the optimization problem.

#### 3.1. Framework

The general framework in Fig. 8 is used in our PSST for problem clarification, which combines self-supervised task and supervised class recognition task in a few-shot setting. We train the feature extractor  $\theta^{sh}$  with both labeled (top branch) and unlabeled (bottom branches) data in a multi-task setting. We use the labeled data to train the object classifier  $\theta^1$  with few-shot classification loss. For the self-supervised task, we sample images from the unlabeled dataset. For example, we generate four rotations for each input image in rotation task, process them with  $\theta^{sh}$  and train the rotation classifier  $\theta^2$  with the self-supervised loss. The pipeline for other self-supervised tasks is analog to this one.

#### 3.2. Multi-Objective FSAL

Our goal is to improve few-shot learning performance via self-supervised training. Different from previous works using a weighted sum of loss functions for few-shot auxiliary learning with self-supervised learning [11, 16], we cast few-shot auxiliary learning as multi-objective optimization rather than a weighted sum of loss function.

We consider the few-shot auxiliary learning over an input space  $\mathcal{X}$  and a collection of task spaces  $\{\mathcal{Y}^m\}_{m \in [M]}$ , such that a large dataset of independent and identically distributed (i.i.d.) data points  $\{\mathbf{x}_i, y_i^1, \dots, y_i^M\}_{i \in [N]}$  is given, where  $M$  is the number of tasks,  $N$  is the number of data points, and  $y_i^m$  is the label of the  $m^{th}$  task for the  $i^{th}$  data point. As shown in Fig. 8, we further consider a parametric hypothesis class per task as  $f^m(\mathbf{x}; \theta^{sh}, \theta^m) : \mathcal{X} \rightarrow \mathcal{Y}^m$ , such that some parameters ( $\theta^{sh}$ ) are shared between tasks and others ( $\theta^m$ ) are task-specific. Define the task-specific loss function by  $\mathcal{L}_m(\cdot, \cdot) : \mathcal{Y}^m \times \mathcal{Y}^m \rightarrow \mathbb{R}^+$ .

Previous works [11, 16] are to optimize a proxy objective that minimizes a weighted linear combination of per-task losses:

$$\min_{\theta} L(\theta) = \sum_{m=1}^M \omega_m L_m(\theta^{sh}, \theta^m), \quad (1)$$

where  $\omega_m$  is the weight for the  $m$ -th task, and  $L_m(\theta^{sh}, \theta^m)$  is the empirical loss of the task  $m$ , defined as  $L_m(\theta^{sh}, \theta^m) \triangleq \frac{1}{N} \sum_{i=1}^N L_m(f^m(\mathbf{x}_i; \theta^{sh}, \theta^m), y_i^m)$ . This approach is simple and straightforward, however, it has some drawbacks which have been pointed out by many recent works [27, 28].

In a typical few-shot auxiliary learning application, the weight  $\omega_m$  is needed to be assigned manually before optimization, and the overall performance is highly dependent on the assigned weights. Choosing a proper weight vector could be very difficult even for an expert. To accurately model the trade-off between tasks, which is beyond what a linear combination can achieve, multi-objective optimization is widely used in recent works [27, 28].

Previous works focus on weighted summation due to its intuitively appealing [11, 16, 7], however, these works typically require either an expensive grid search over various scalings or the use of some heuristics. Recent work formulates the weighted summation as multi-objective optimization, which optimizes a collection of possibly conflicting objectives [27]. By adopting this, we reformulate our few-shot auxiliary learning as multi-objective optimization problem with a vector-valued loss  $\mathcal{L}$ :

$$\min_{\theta} \mathcal{L}(\theta) = \min_{\theta} (\mathcal{L}_1(\theta^{sh}, \theta^1), \dots, \mathcal{L}_M(\theta^{sh}, \theta^M))^T, \quad (2)$$

where  $\theta = \{\theta^{sh}, \theta^1, \dots, \theta^M\}$ . The goal of multi-objective optimization is to reach Pareto optimality.

**Definition 1** (Pareto dominance): A solution  $\theta$  dominates a solution  $\bar{\theta}$  if  $\mathcal{L}_m(\theta^{sh}, \theta^m) \leq \mathcal{L}_m(\bar{\theta}^{sh}, \bar{\theta}^m)$  for all tasks  $m$  and  $\mathcal{L}(\theta^{sh}, \theta^1, \dots, \theta^M) \neq \mathcal{L}(\bar{\theta}^{sh}, \bar{\theta}^1, \dots, \bar{\theta}^M)$ .

**Definition 2** (Pareto optimality): A solution  $\theta^*$  is called Pareto optimal if there exists no solution  $\theta$  that dominates  $\theta^*$ . The set of Pareto optimal solutions is called the Pareto front ( $\mathcal{P} = \{\mathcal{L}(\theta^*)\}_{\theta^* \in \mathcal{P}_{\theta^*}}$ ).

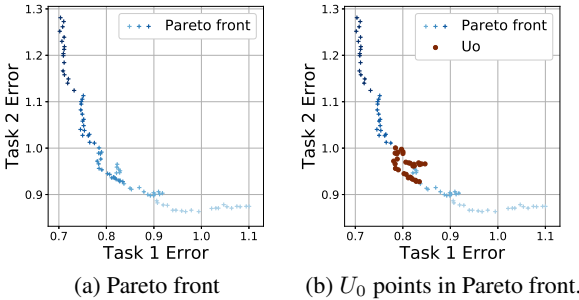


Figure 3: The convergence behaviors of PSST. Each  $U_0$  point is the solution of PSST from different initial parameters of neural network. The proposed PSST successfully find  $U_0$  in the balance space that maximizes the overall performance of two tasks.

### 3.3. Optimization of Multi-Objective FSAL

#### 3.3.1 Gradient-based multi-objective optimization

Many gradient-based methods have been proposed for solving multi-objective optimization problems [15, 27]. Fliege and Svaiter [14] have proposed a simple gradient-based method, which is a generalization of a single objective steepest descent algorithm. The update rule of the algorithm is  $\theta_{t+1} = \theta_t + \eta d_t$ , where  $\eta$  is the step size and the search direction  $d_t$  is obtained as follows:

$$(d_t, \alpha_t) = \arg \min_{d \in R^M, \alpha \in R} \alpha + \frac{1}{2} \|d\|^2, \quad (3)$$

s.t.  $\nabla \mathcal{L}_m(\theta_t)^T d \leq \alpha, m = 1, \dots, M.$

The solutions of the above problem will satisfy:

**Lemma 1** [14]: Let  $(d^k, \alpha^k)$  be the solution of problem in Eq. 3. If  $\theta_t$  is Pareto optimal, then  $d_t = 0 \in \mathbb{R}^n$  and  $\alpha_t = 0$ . If  $\theta_t$  is not Pareto optimal, then

$$\alpha_t \leq -(1/2) \|d_t\|^2 < 0, \quad (4)$$

$\nabla \mathcal{L}_m(\theta_t)^T d_t \leq \alpha_t, m = 1, \dots, M,$

where  $\theta$  is called Pareto optimal if no other solution in its neighborhood has better value in all objective functions. In other words, if  $d_t = 0$ , no direction can improve the performance for all tasks at the same time. If we want to improve the performance for one specific task, another task will be deteriorated (e.g.,  $\exists m, \nabla \mathcal{L}_m(\theta_t)^T d_t > 0$ ). Therefore, the current solution is a Pareto optimal point. When  $d_t \neq 0$ , we have  $\nabla \mathcal{L}_m(\theta_t)^T d_t < 0, m = 1, \dots, M$ , which means  $d_t$  is a valid descent direction for all tasks. The current solution should be updated along the obtained direction  $\theta_{t+1} = \theta_t + \eta d_t$ , and will be stopped once a feasible solution is found.

As shown in Fig. 3, using gradient-based method in Eq. 3 to solve multi-objective optimization problems, the interaction between gradients within their shared parameters is

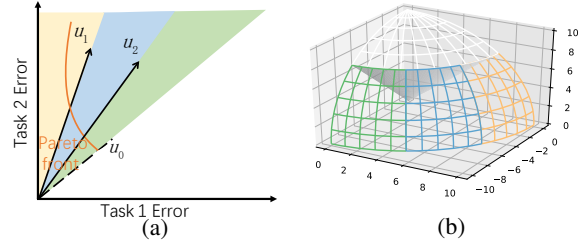


Figure 4: Illustrative examples of preference region in (a) 2 tasks (b) 3 tasks, where the white space will not be explored.

balanced, which leads to balanced performances for different tasks. Thus, the solutions where given multiple different initial parameters achieve balanced performances for different tasks, and these solutions are in the space where different tasks are balanced.

#### 3.3.2 Optimization in preference region

Decomposition-based multi-objective evolutionary algorithm [42, 49] is one of the most popular gradient-free multi-objective optimization methods, which decomposes a multi-objective optimization problem into  $K$  subproblems via preference vectors  $\{\mathbf{u}_1, \mathbf{u}_2, \dots, \mathbf{u}_K\}$  in  $R_+^M$  and solves them simultaneously. The preference vectors in these methods are handcrafted, and all subproblems are solved. However, in few-shot auxiliary learning, we focus on the main task, the challenge lies in how to identify the preference region where the main task achieves the best performance.

Because of the distinct optimization of different tasks, it is difficult to directly determine the space where the main task achieves optimal performance. Therefore, the goal is to exclude the parts that are not interested, where the auxiliary tasks hamper the performance of the main task. We try to find the space where distinct tasks are balanced. If the performance of the main task is not better than the balanced performance of the main task, we will remove this part in the space. We identify and empirically demonstrate the solution of gradient-based optimization method for multi-objective optimization lying in the set where the overall performance of different tasks are balanced. An illustrative example is shown in Fig. 4.

Assuming the best overall performance is achieved when all tasks are balanced, we state that if the performance of the main task is no better than the balanced performance of the main task, the auxiliary tasks hamper the main task. Let  $\rho(\theta)$  be the proportion of performance in the main task over the performance of all auxiliary tasks in  $\theta$ , i.e.,  $\rho(\theta) = \frac{\mathcal{L}_1(\theta)}{\sum_{m=2}^M \mathcal{L}_m(\theta)}$ , we formalize the result as follows.

**Lemma 2:** If  $\theta_{\pi 0}^*$  achieves the best overall performance, i.e.  $\min_{\theta} \sum_{m=1}^M \mathcal{L}_m(\theta) = \sum_{m=1}^M \mathcal{L}_m(\theta_{\pi 0}^*)$ , and a better performance of the main task can be achieved in  $\theta'$ , i.e.,

$\mathcal{L}_1(\theta') < \mathcal{L}_1(\theta_{\pi 0}^*)$ , then  $\rho(\theta') < \rho(\theta_{\pi 0}^*)$ . The proof of Lemma 2 can be found in supplemental materials.

Noting that  $\rho(\theta) = \rho(\theta_{\pi 0}^*)$  is a hyperplane dividing the objective space into two parts, we remove the part satisfying  $\rho(\theta) > \rho(\theta_{\pi 0}^*)$ , and further divide the remaining part satisfying  $\rho(\theta) \leq \rho(\theta_{\pi 0}^*)$  into different regions with preference vectors to avoid residual error accumulation, which is detailed in Section 3.4. An illustrate example is shown in Fig. 4, the white space stands for  $\rho(\theta) > \rho(\theta_{\pi 0}^*)$ .

**Subproblem Decomposition.** With the solution  $\theta_{\pi 0}^*$ , we have  $\mathcal{L}(\theta_{\pi 0}^*) = [\mathcal{L}_1(\theta_{\pi 0}^*), \mathcal{L}_2(\theta_{\pi 0}^*), \dots, \mathcal{L}_M(\theta_{\pi 0}^*)]^T$ . In a 2-D space,  $\rho(\theta) = \rho(\theta_{\pi 0}^*)$  is a line, its direction vector is well defined. In a M-dimentional (M-D) space ( $M \geq 3$ ),  $\rho(\theta) = \rho(\theta_{\pi 0}^*)$  is a hyperplane. This hyperplane will intersects the coordinate planes and form some lines. We define the direction vectors of  $\rho(\theta) = \rho(\theta_{\pi 0}^*)$  in M-D space as the direction vectors of the intersections formed by the hyperplane and coordinate planes. Coordinate plane is 2-D space, which corresponding two tasks with the name “two tasks scenario” comes from this place. Let unit vector  $u_0$  be one of the direction vector of  $\rho(\theta) = \rho(\theta_{\pi 0}^*)$  for two-task scenario, we have  $u_0 = (\cos \pi_0, \sin \pi_0)$ , where  $\cos \pi_0 = \frac{e_1 \mathcal{L}(\theta_{\pi 0}^*)}{\|T_2 \mathcal{L}(\theta_{\pi 0}^*)\|_2}$  and  $T_m = I - e^{mm}$ . Here,  $e^{mm}$  is a single-entry matrix, i.e. the  $m$ th element in the  $m$ th column being one and the rest elements being zero;  $e_1 = (1, 0)^T$ ;  $I$  is an identity matrix. Given the  $u_0$ , we further decompose the auxiliary problem into  $K$  subproblems with a set of unit preference vectors  $\{u_1, u_2, \dots, u_K\}$ , for the preference vector  $u_i$ :

$$\begin{aligned} u_i &= (\cos \pi_i, \sin \pi_i), \\ \text{s.t. } \pi_i &= \frac{i}{K} \left( \frac{\pi}{2} - \pi_0 \right) + \pi_0, i = 1, \dots, K, \end{aligned} \quad (5)$$

where the derivation and proof of the preference vectors can be found in supplemental materials, followed by a further discussion on preference vector in multiple tasks.

Suppose all objectives in the multi-objective optimization are non-negative, the multi-objective subproblem corresponding to the preference vector  $u_i$  and  $u_{i+1}$  is:

$$\begin{aligned} \min_{\theta} \mathcal{L}(\theta) &= (\mathcal{L}_1(\theta), \mathcal{L}_2(\theta), \dots, \mathcal{L}_M(\theta))^T, \\ \text{s.t. } u_i e_1^T &\leq \frac{e_1 \mathcal{L}(\theta)}{\|T_2 \mathcal{L}(\theta)\|_2} \leq u_{i+1} e_1^T. \end{aligned} \quad (6)$$

The subproblem Eq. 6 can be further reformulated as:

$$\begin{aligned} \min_{\theta} \mathcal{L}(\theta) &= (\mathcal{L}_1(\theta), \mathcal{L}_2(\theta), \dots, \mathcal{L}_M(\theta))^T, \\ \text{s.t. } \mathcal{Q}_i(\theta) &= \frac{e_1 \mathcal{L}(\theta)}{\|T_2 \mathcal{L}(\theta)\|_2} - u_{i+1} e_1^T \leq 0, \\ \mathcal{R}_i(\theta) &= u_i e_1^T - \frac{e_1 \mathcal{L}(\theta)}{\|T_2 \mathcal{L}(\theta)\|_2} \leq 0. \end{aligned} \quad (7)$$

The proof can be found in supplemental materials.

**Preferred Pareto Optimality.** To solve the constrained multi-objective subproblem with preference vector  $u_i$  and  $u_{i+1}$ , we need to find an initial solution which is feasible

or at least satisfies most constraints. For a randomly generated solution  $\theta$ , we define the index set of all activated constraints as  $\mathcal{K}_\epsilon(\theta) = \{k \mid \mathcal{Q}_k(\theta) \geq -\epsilon, k = 0, \dots, K-1\}$  and  $\mathcal{J}_\epsilon(\theta) = \{j \mid \mathcal{R}_j(\theta) \geq -\epsilon, j = 0, \dots, K-1\}$ , where  $\epsilon$  is a threshold. We can find a valid descent direction  $d_t$  to reduce the value of all activated constraints by solving:

$$\begin{aligned} (d_t, \alpha_t) &= \arg \min_{d \in R^M, \alpha \in R} \alpha + \frac{1}{2} \|d\|_2^2, \\ \text{s.t. } \nabla \mathcal{L}_m(\theta_t)^T d &\leq \alpha, m = 1, \dots, M, \\ \nabla \mathcal{Q}_k(\theta_t)^T d &\leq \alpha, k \in \mathcal{K}_\epsilon(\theta_t), \\ \nabla \mathcal{R}_j(\theta_t)^T d &\leq \alpha, j \in \mathcal{J}_\epsilon(\theta_t). \end{aligned} \quad (8)$$

The valid descent direction can be found by solving the constrained optimization problem in Eq. 8. However, the optimization problem itself is not scalable well for high dimensional decision space especially in deep neural networks. To solve the constrained optimization problem, we propose a scalable optimization method. Inspired by [14], we first rewrite the optimization problem Eq. 8 in its dual form. Based on the KKT conditions, we have the update direction as

$$\begin{aligned} d_t(\omega_m, \beta_k, \gamma_j) &= - \left( \sum_{m=1}^M \omega_m \nabla \mathcal{L}_m(\theta_t) \right. \\ &\quad \left. + \sum_{k \in \mathcal{K}_\epsilon(\theta_t)} \beta_k \nabla \mathcal{Q}_k(\theta_t) + \sum_{j \in \mathcal{J}_\epsilon(\theta_t)} \gamma_j \nabla \mathcal{R}_j(\theta_t) \right), \end{aligned} \quad (9)$$

where  $\omega_m \geq 0, \beta_k \geq 0$  and  $\gamma_j \geq 0$  are the Lagrange multipliers for the linear inequality constraints. Therefore, the dual problem is:

$$\begin{aligned} \max_{\omega_m, \beta_k, \gamma_j} & -\frac{1}{2} \|d_t(\omega_m, \beta_k, \gamma_j)\|_2^2, \\ \text{s.t. } \sum_{m=1}^M \omega_m + \sum_{k \in \mathcal{K}_\epsilon(\theta_t)} \beta_k + \sum_{j \in \mathcal{J}_\epsilon(\theta_t)} \gamma_j &= 1, \\ \forall m &= 1, \dots, M, \forall k \in \mathcal{K}_\epsilon(\theta_t), \forall j \in \mathcal{J}_\epsilon(\theta_t), \\ \omega_m &\geq 0, \beta_k \geq 0, \gamma_j \geq 0. \end{aligned} \quad (10)$$

The details of derivations and proofs are shown in supplemental materials.

For the above problem, the decision space is no longer the parameter space, and it becomes the objective and constraint space. For a multi-objective optimization problem with three objective functions and seven activated constraints, the dimension of problem in Eq. 10 is ten, which is significantly smaller than the dimension of problem in Eq. 8 which is very large and could be more than a million.

As shown in Fig. 4, the preference vectors divide the objective space into different sub-regions, and with the restricted of  $u_0$ , the space where auxiliary tasks hamper the performance of the main task will not be considered, the computation at training time decreases with a smaller exploration space. The set of solutions for all subproblems would be in different sub-regions and represent different trade-offs among the tasks.

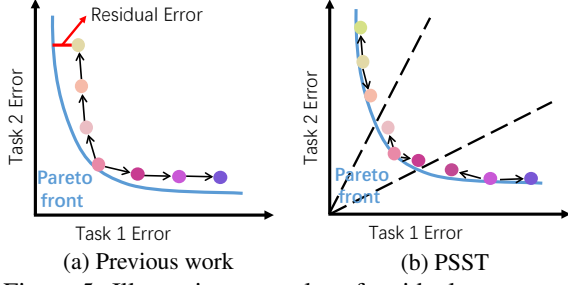


Figure 5: Illustrative examples of residual error accumulation problem in previous Pareto exploration, and PSST alleviate this issue by preferred Pareto exploration.

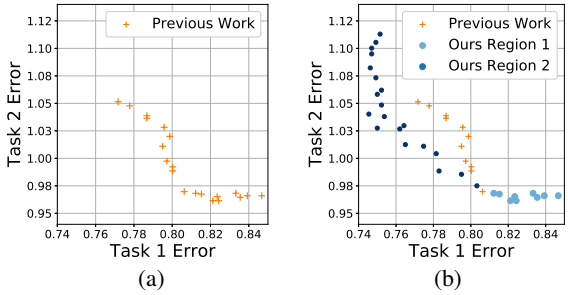


Figure 6: Residual error comparison between (a) previous work and (b) PSST, details in Section 4.

### 3.4. Preferred Pareto Exploration

Pareto exploration aims at finding several Pareto solutions. Different from the grid search in the weighted sum of objectives, the Pareto exploration is more efficiency in finding Pareto solutions [28]. However, previous Pareto exploration has the residual error accumulation problem as shown in Figs. 5 and 6. To avoid such residual error accumulation, we explore the sub-regions instead of the whole region.

**Find a Pareto solution.** Firstly, our preferred Pareto exploration takes random parameters of neural network  $\theta$  as input, and find a Pareto solution  $\theta^*$  via direction  $d_t$  in Eq.9.

**Find gradient on the tangent plane at  $\theta^*$ .** Secondly, once a Pareto solution  $\theta^*$  is found, we explore its local Pareto set by spawning new points  $\theta_t$ .

**Lemma 3 [23]:** If  $\theta^*$  is Pareto optimal, there will be a  $\lambda \in \mathbb{R}^M$  such that  $\lambda_m \geq 0$ ,  $\sum_{m=1}^M \lambda_m = 1$ , and  $\sum_{m=1}^M \lambda_m \nabla \mathcal{L}_m(\theta^*) = 0$ .

**Proposition [22]:** Assuming that  $\mathcal{L}(\theta^*)$  is smooth and  $\theta^*$  is Pareto optimal, consider any smooth curve  $\theta_{(x)} : (-\epsilon, \epsilon) \rightarrow \mathbb{R}^M$  in the Pareto set and passing  $\theta^*$  at  $x = 0$ , i.e.,  $\theta_{(0)} = \theta^*$ , then for  $\exists \beta \in \mathbb{R}^M$  we have:

$$\mathbf{H}(\theta^*) \frac{d\theta}{dx}(0) = \nabla \mathcal{L}(\theta^*)^\top \beta, \quad (11)$$

where  $\mathbf{H}(\theta^*) = \sum_{m=1}^M \lambda_m \nabla^2 \mathcal{L}_m(\theta^*)$ , and we use  $\frac{d\theta}{dx}(0)$  as the update direction and calculate  $\theta_1 = \theta_{(0)} + \eta \frac{d\theta}{dx}(0)$ . Solving such problem requires an efficient matrix solver.

---

### Algorithm 1 Few shot Learning via Pareto Self-supervised Training

---

```

1: Input: A random initial neural network  $\theta$ .
2: Find a Pareto solution  $\theta_0^*$  via direction  $d_t$  in Eq. 3
3: Find  $\pi_0 = \arccos \frac{e_1 \mathcal{L}(\theta_0^*)}{\|T_2 \mathcal{L}(\theta_0^*)\|_2}$ ,  $u_0 = (\cos \pi_0, \sin \pi_0)$ .
4: Calculate vectors  $\{u_1, u_2, \dots, u_K\}$  via Eq. 12.
5: for all  $i = 0$  to  $K - 1$  do
6:   Randomly generate parameters  $\theta^{(i)}$ .
7:   Find Pareto solution  $\theta^{(i)*}$  via direction  $d_t$  in Eq. 9.
8:    $s_i \leftarrow \text{PreferredParetoExploration } (\theta^{(i)*})$ 
9: end for
10: Output: The set of solutions for all subproblems  $\{s_i \mid i = 1, \dots, K\}$ .

```

---

Similar to [28], we use Krylov subspace iteration methods. The details of derivations and proofs are shown in supplemental materials, followed the method of obtain  $\lambda$ .

#### Explore a set of Pareto solutions (line 8 in Algorithm 1).

To explore a set of Pareto solutions based on  $\theta^*$  in the region between  $u_i$  and  $u_{i+1}$ , we initialize a queue  $q \leftarrow [\theta^*]$  and a set  $s \leftarrow [\theta^*]$ . Given a Pareto solution  $\theta^*$ , with gradient  $\frac{d\theta}{dx}(0)$  on the tangent plane at  $\theta^*$ , we can have  $\theta_1 = \theta^* + \eta \frac{d\theta}{dx}(0)$ . Here,  $\theta_1$  is the first-order approximation of a Pareto solution close to  $\theta^*$ , and we can have a Pareto solution  $\theta_1^*$  via direction  $d_t$  in Eq.9. The queue and set collect all the Pareto solutions:  $q \leftarrow [\theta_1^*]$  and  $s \leftarrow [\theta_1^*]$ . Once we cannot find any approximate point at  $\theta^*$ , we remove  $\theta^*$  from queue  $q$ , and do the same to all points in the queue  $q$ . Thus, we explore all the Pareto solutions in the region between  $u_i$  and  $u_{i+1}$ . Pareto solutions in all regions are saved in set  $s$ . The Pareto solution which has the best performance in the main task will be the final solution for a specific few-shot task. We summarize the PSST in Algorithm 1.

To summarize, the efficiency of our exploration algorithm comes from two sources: exploration on the tangent plane and termination with restricted preference region. The time cost of getting one tangent direction is  $O(kn)$ ,  $k$  is the iteration and  $n$  is the size of input data, which scales linearly to the network size.

## 4. Experiments

We design two experiments, which we call the sufficiency and necessity tests, to show the effectiveness and efficiency of our proposed PSST.

In the necessity test, which focuses on demonstrate the effectiveness of our proposed PSST in few-shot auxiliary learning, we compare our approach with prior few-shot methods on the MiniImageNet and CIFAR-FS datasets respectively. We call this experiment the necessity test as we use this experiment to establish that our proposed PSST, multi-objective optimization strategies rather than

Models	Backbone	1-shot	5-shot
MetaOptNet [26]	ResNet-12	62.64 $\pm$ 0.61	78.63 $\pm$ 0.46
	ResNet-12	62.93 $\pm$ 0.63	79.63 $\pm$ 0.47
	ResNet-12	<b>64.05 <math>\pm</math> 0.49</b>	<b>80.24 <math>\pm</math> 0.45</b>
CC [17]	WRN-28-10	61.09 $\pm$ 0.44	78.43 $\pm$ 0.33
	WRN-28-10	60.71 $\pm$ 0.46	77.64 $\pm$ 0.34
	WRN-28-10	<b>63.26 <math>\pm</math> 0.44</b>	<b>80.05 <math>\pm</math> 0.34</b>
+ rot, (BF3S [16])	WRN-28-10	62.93 $\pm$ 0.45	79.87 $\pm$ 0.33
	WRN-28-10	<b>64.16 <math>\pm</math> 0.44</b>	<b>80.64 <math>\pm</math> 0.32</b>
	ResNet-18	54.16 $\pm$ 0.82	73.68 $\pm$ 0.65
ProtoNet [39]	ResNet-18	57.92 $\pm$ 0.58	76.00 $\pm$ 0.58
	ResNet-18	<b>59.28 <math>\pm</math> 0.46</b>	<b>77.18 <math>\pm</math> 0.43</b>
	ResNet-18	58.35 $\pm$ 0.50	76.20 $\pm$ 0.53
+ jig, (SSFSL [40])	ResNet-18	<b>59.34 <math>\pm</math> 0.45</b>	<b>77.27 <math>\pm</math> 0.43</b>
	ResNet-18	58.84 $\pm$ 0.49	76.60 $\pm$ 0.52
	ResNet-18	<b>59.52 <math>\pm</math> 0.46</b>	<b>77.43 <math>\pm</math> 0.46</b>

Table 1: Average accuracy (%) comparison with 95 confidence intervals before and after incorporating PSST into existing methods on MiniImageNet. Best results are displayed in boldface.

grid search in the weighted sum of objectives are indeed the source of efficiency in our method.

In the sufficiency test, we consider previous Pareto exploration method to show that our PSST is a fast and effective method. We call this experiment the sufficiency test as it demonstrates our method is able to quickly explore Pareto sets and Pareto front in few-shot auxiliary learning.

**Datasets.** We perform experiments on two few-shot datasets for necessity test: MiniImageNet [44] and CIFAR-FS [1]. MultiMNIST [36] is used for sufficiency test. Mini-ImageNet consists of 100 classes randomly picked from the ImageNet dataset [35] (i.e., 64 base classes, 16 validation classes, and 20 novel test classes); each class has 600 images with size  $84 \times 84$  pixels. CIFAR-FS is a few-shot dataset created by dividing the 100 classes of CIFAR-100 into 64 base classes, 16 validation classes, and 20 novel test classes. The images in this dataset have size  $32 \times 32$  pixels. Please refer to our supplemental materials for more information about the network architectures, task descriptions, and implementation details in each dataset.

**Evaluation metrics.** Few-shot classification algorithms are evaluated based on the classification accuracy in their testing stage (when the learned classifier is applied to test images from the novel classes). Specifically, a large number of  $N_n$ -way  $K$ -shot tasks are sampled from the available set of novel classes. Each task is created by randomly selecting  $N_n$  novel classes from the available test (validation) classes and then within the selected classes randomly selecting  $K$  train and  $M$  test images per class (making sure that train and test images do not overlap). The classification accuracy is measured on the  $N_n \times M$  test images and is averaged over all the sampled few-shot tasks. Except otherwise stated, for all experiments we use  $M = 15$ ,  $N_n = 5$ , and  $K = 1$  or  $K = 5$  (1-shot and 5-shot settings respectively).

**Reduce the task conflict.** To verify the effectiveness of our proposed PSST, we embed it into three self-supervised

Models	Backbone	1-shot	5-shot
MAML [13]	Conv-4-64	48.70 $\pm$ 1.84	63.10 $\pm$ 0.92
Prototypical Nets [39]	Conv-4-64	49.42 $\pm$ 0.78	68.20 $\pm$ 0.66
R2-D2 [1]	Conv-4-64	48.70 $\pm$ 0.60	65.50 $\pm$ 0.60
LwoF [17]	Conv-4-64	56.20 $\pm$ 0.86	72.81 $\pm$ 0.62
BF3S [16]	Conv-4-64	54.83 $\pm$ 0.43	71.86 $\pm$ 0.33
RelationNet [41]	Conv-4-64	50.40 $\pm$ 0.80	65.30 $\pm$ 0.70
GNN [37]	Conv-4-64	50.30	66.40
TADAM [31]	ResNet-12	58.50 $\pm$ 0.30	76.70 $\pm$ 0.30
Munkhdalai et al. [30]	ResNet-12	57.10 $\pm$ 0.70	70.04 $\pm$ 0.63
SNAIL [29]	ResNet-12	55.71 $\pm$ 0.99	68.88 $\pm$ 0.92
Shot-Free [34]	ResNet-12	59.04	77.64
MetaOptNet [26]	ResNet-12	62.64 $\pm$ 0.61	78.63 $\pm$ 0.46
Qiao et al. [33]	WRN-28-10	61.76 $\pm$ 0.08	77.59 $\pm$ 0.12
BF3S [16]	WRN-28-10	62.93 $\pm$ 0.45	79.87 $\pm$ 0.33
Su et al. [40]	WRN-28-10	60.43 $\pm$ 0.58	76.60 $\pm$ 0.29
AWGIM [19]	WRN-28-10	63.12 $\pm$ 0.08	78.40 $\pm$ 0.11
PSST	Conv-4-64	57.04 $\pm$ 0.51	73.17 $\pm$ 0.48
PSST	WRN-28-10	<b>64.16 <math>\pm</math> 0.44</b>	<b>80.64 <math>\pm</math> 0.32</b>

Table 2: Few-shot image classification average accuracy (%) comparison with state-of-the-arts with 95% confidence intervals on MiniImageNet.

Models	Backbone	1-shot	5-shot
Prototypical Nets [39]	Conv-4-64	62.82 $\pm$ 0.32	79.59 $\pm$ 0.24
MAML [13]	Conv-4-64	58.90 $\pm$ 1.90	71.50 $\pm$ 1.00
RelationNet [41]	Conv-4-64	55.00 $\pm$ 1.00	69.30 $\pm$ 0.80
BF3S [16]	Conv-4-64	63.45 $\pm$ 0.31	79.79 $\pm$ 0.24
GNN [37]	Conv-4-64	61.90	75.30
R2-D2 [1]	Conv-4-64	60.00 $\pm$ 0.70	76.10 $\pm$ 0.60
Shot-Free [34]	ResNet-12	69.20 $\pm$ 0.40	84.70 $\pm$ 0.40
MetaOptNet [26]	ResNet-12	72.00 $\pm$ 0.70	84.20 $\pm$ 0.50
BF3S [16]	WRN-28-10	76.09 $\pm$ 0.30	87.83 $\pm$ 0.21
PSST	Conv-4-64	64.37 $\pm$ 0.33	80.42 $\pm$ 0.32
PSST	WRN-28-10	<b>77.02 <math>\pm</math> 0.38</b>	<b>88.45 <math>\pm</math> 0.35</b>

Table 3: Few-shot image classification average accuracy (%) comparison with state-of-the-arts with 95% confidence intervals on CIFAR-FS.

tasks : location prediction (loc), rotation prediction (rot) and jigsaw puzzle (jig), and three widely used meta-learning

Method	BF3S [16]	PSST	
Number of Solutions	1	10	1
Time (1 iteration)	1.02s	1.02s	1.05s
Iterations ( $\times 10^3$ )	24	249	24

Table 4: Training time on the same GPU device. Multiple solutions are based on different trade-offs.

baselines: MetaOptNet [26], Cosine Classifier (CC) [17] and ProtoNet [39]. Table 1 shows that for all cases, incorporating PSST leads to a significant improvement which demonstrates the effectiveness of our PSST. Specifically, the performance gain is 5.36% on 1-shot and 3.75% on 5-shot in ProtoNet with rotation prediction task and jigsaw puzzle task. Particularly, the performance of BF3S method with location prediction task is lower than that without location prediction task in both 1-shot and 5-shot image classification task, which is caused by the *task conflict*. Incorporating PSST leads to a significant improvement. We believe the reason is that location prediction task hampers the performance of BF3S, and our PSST effectively find a proper trade-off to reduce the task conflict between image classification and location prediction.

**Comparison with prior works.** In Tables 2 and 3, we compare our approach with prior few-shot methods on the MiniImageNet and CIFAR-FS datasets respectively. For our approach, we use CC and rotation prediction task, which gave the best results. In all cases we achieve state-of-the-art results surpassing prior methods.

**Training time analysis.** To further show the efficiency of PSST, we compare our approach with BF3S on the same GPU device as shown in Table 4. For a single solution, the training time of two method is close. For multiple solutions with different trade-offs, *e.g.* 10 solutions, BF3S with different weights via grid search needs  $249 \times 10^3$  iterations, and PSST only needs  $60 \times 10^3$  iterations, which is much faster than BF3S due to the effective preferred Pareto exploration.

In our sufficiency test, to evaluate our preferred Pareto exploration, similar to previous Pareto exploration work [28], we pick a subset of 2048 images from MultiMNIST.

**Effective region decomposition.** To demonstrate the effectiveness of our PSST, we assign PSST different initial parameters of neural network, and the results shows in Fig. 3. All  $u_0$  points are in the balance space where the overall performance of two tasks achieve good performance, however, which may not be the best performance for a specific task. Given the  $u_0$  points in the balance space, we can remove the space where the auxiliary tasks hamper the performance of the main task. The smaller exploration region is one of the sources of efficiency in our method.

**Decrease residual error.** To analyze how PSST decreases residual error, we record the exploration trajectories of both previous method and our PSST as shown in

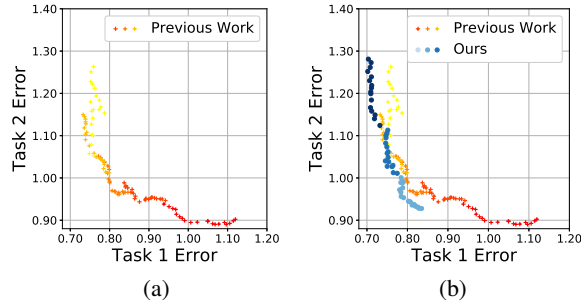


Figure 7: Performance comparison between (a) previous Pareto exploration and (b) our PSST.

Fig. 6. Compared with previous method, our trajectories are pushed towards its lower left, indicating a better approximated Pareto front. We believe the reason is that the first-order approximation of a Pareto solution is closer to the Pareto front, and the exploration of  $\theta^*$  is restricted in the sub-region with less residual error.

**Performance comparison of Pareto exploration.** As shown in Fig. 7, our method achieves a better performance on the main task with fewer explorations. Our trajectories are pushed towards its lower left, indicating a better approximated Pareto front. The training time of each iteration is the same for both methods, our PSST achieves better performance with 78 iterations, and previous work needs 130 iterations, which demonstrates both effectiveness and efficiency of our PSST. The efficiency of PSST is from less exploration space and the effectiveness is from the decreasing residual error.

## 5. Conclusion

In this paper, we study the problem of task conflict in few-shot auxiliary learning. We propose a novel Pareto self-supervised training to reduce the task conflict in few-shot auxiliary learning. We explicitly cast few-shot auxiliary learning as multi-objective optimization, with the overall objective of finding a Pareto optimal solution. We decompose the few-shot auxiliary problem into several constrained multi-objective subproblems with different trade-off preferences allowing better exploration of the frontier. Experiments demonstrate both efficiency and effectiveness of our proposed PSST: where the efficiency of PSST is from the less exploration space and the effectiveness is from the decreasing residual error.

## 6. Acknowledgments

The authors gratefully acknowledge funding support from the Westlake University and Bright Dream Joint Institute for Intelligent Robotics.

## References

[1] Luca Bertinetto, João F. Henriques, Philip H. S. Torr, and Andrea Vedaldi. Meta-learning with differentiable closed-form solvers. In *7th International Conference on Learning Representations, ICLR 2019, New Orleans, LA, USA, May 6-9, 2019*, 2019. 2, 7

[2] Piotr Bojanowski and Armand Joulin. Unsupervised learning by predicting noise. In *Proceedings of the 34th International Conference on Machine Learning - Volume 70*, pages 517–526, 2017. 1, 2

[3] Fabio M Carlucci, Antonio D’Innocente, Silvia Bucci, Barbara Caputo, and Tatiana Tommasi. Domain generalization by solving jigsaw puzzles. In *Proceedings of the IEEE Conference on Computer Vision and Pattern Recognition*, pages 2229–2238, 2019. 2

[4] Mathilde Caron, Piotr Bojanowski, Julien Mairal, and Armand Joulin. Unsupervised pre-training of image features on non-curated data. In *Proceedings of the IEEE International Conference on Computer Vision*, pages 2959–2968, 2019. 2

[5] Zhengyu Chen and Donglin Wang. Multi-initialization meta-learning with domain adaptation. In *2021 IEEE International Conference on Acoustics, Speech and Signal Processing, ICASSP 2021*, 2021. 2

[6] Zhengyu Chen, Donglin Wang, and Shiqian Yin. Improving cold-start recommendation via multi-prior meta-learning. In *43rd European Conference on Information Retrieval, ECIR 2021*, 2021. 2

[7] Zhengyu Chen, Ziqing Xu, and Donglin Wang. Deep transfer tensor decomposition with orthogonal constraint for recommender systems. In *The Thirty-Fifth AAAI Conference on Artificial Intelligence, AAAI 2021*, 2021. 3

[8] Kalyanmoy Deb. *Multi-objective optimization using evolutionary algorithms*. Wiley-Interscience series in systems and optimization. Wiley, 2001. 2

[9] Carl Doersch, Abhinav Gupta, and Alexei A Efros. Unsupervised visual representation learning by context prediction. In *Proceedings of the IEEE international conference on computer vision*, pages 1422–1430, 2015. 2, 16

[10] Alexey Dosovitskiy, Jost Tobias Springenberg, Martin Riedmiller, and Thomas Brox. Discriminative unsupervised feature learning with convolutional neural networks. In *Advances in neural information processing systems*, pages 766–774, 2014. 2

[11] Nikita Dvornik, Julien Mairal, and Cordelia Schmid. Diversity with cooperation: Ensemble methods for few-shot classification. In *2019 IEEE/CVF International Conference on Computer Vision, ICCV 2019, Seoul, Korea (South), October 27 - November 2, 2019*, 2019, pages 3722–3730, 2019. 3

[12] Thomas Elsken, Jan Hendrik Metzen, and Frank Hutter. Efficient multi-objective neural architecture search via lamarckian evolution. In *International Conference on Learning Representations*, 2018. 2

[13] Chelsea Finn, Pieter Abbeel, and Sergey Levine. Model-agnostic meta-learning for fast adaptation of deep networks. In *Proceedings of the 34th International Conference on Machine Learning, ICML 2017, Sydney, NSW, Australia, 6-11 August 2017*, pages 1126–1135, 2017. 2, 7

[14] Jörg Fliege and Benar Fux Svaiter. Steepest descent methods for multicriteria optimization. *Mathematical Methods of Operations Research*, 51(3):479–494, 2000. 2, 4, 5

[15] Jörg Fliege and A. Ismael F. Vaz. A method for constrained multiobjective optimization based on SQP techniques. *SIAM J. Optim.*, 26(4):2091–2119, 2016. 4

[16] Spyros Gidaris, Andrei Bursuc, Nikos Komodakis, Patrick Pérez, and Matthieu Cord. Boosting few-shot visual learning with self-supervision. In *2019 IEEE/CVF International Conference on Computer Vision, ICCV 2019, Seoul, Korea (South), October 27 - November 2, 2019*, 2019, pages 8058–8067, 2019. 1, 2, 3, 7, 8, 15

[17] Spyros Gidaris and Nikos Komodakis. Dynamic few-shot visual learning without forgetting. In *2018 IEEE Conference on Computer Vision and Pattern Recognition, CVPR 2018, Salt Lake City, UT, USA, June 18-22, 2018*, pages 4367–4375, 2018. 2, 7, 8, 16

[18] Spyros Gidaris, Praveer Singh, and Nikos Komodakis. Unsupervised representation learning by predicting image rotations. In *International Conference on Learning Representations*, 2018. 2, 16

[19] Yiluan Guo and Ngai-Man Cheung. Attentive weights generation for few shot learning via information maximization. In *2020 IEEE/CVF Conference on Computer Vision and Pattern Recognition, CVPR 2020, Seattle, WA, USA, June 13-19, 2020*, pages 13496–13505, 2020. 2, 7

[20] Kaiming He, Haoqi Fan, Yuxin Wu, Saining Xie, and Ross Girshick. Momentum contrast for unsupervised visual representation learning. In *Proceedings of the IEEE/CVF Conference on Computer Vision and Pattern Recognition*, pages 9729–9738, 2020. 1, 2

[21] Daniel Hernández-Lobato, Jose Hernandez-Lobato, Amar Shah, and Ryan Adams. Predictive entropy search for multi-objective bayesian optimization. In

*International Conference on Machine Learning*, pages 1492–1501, 2016. 2

[22] Claus Hillermeier. Generalized homotopy approach to multiobjective optimization. *Journal of Optimization Theory and Applications*, 110(3):557–583, 2001. 6, 17

[23] Claus Hillermeier et al. *Nonlinear multiobjective optimization: a generalized homotopy approach*, volume 135. Springer Science & Business Media, 2001. 6, 17

[24] Alexander Kolesnikov, Xiaohua Zhai, and Lucas Beyer. Revisiting self-supervised visual representation learning. In *Proceedings of the IEEE conference on Computer Vision and Pattern Recognition*, pages 1920–1929, 2019. 16

[25] Hankook Lee, Sung Ju Hwang, and Jinwoo Shin. Self-supervised label augmentation via input transformations. In *Proceedings of Machine Learning and Systems 2020*, pages 3537–3547. 2020. 7

[26] Kwonjoon Lee, Subhransu Maji, Avinash Ravichandran, and Stefano Soatto. Meta-learning with differentiable convex optimization. In *IEEE Conference on Computer Vision and Pattern Recognition, CVPR 2019*, pages 10657–10665, 2019. 7, 8

[27] Xi Lin, Hui-Ling Zhen, Zhenhua Li, Qingfu Zhang, and Sam Kwong. Pareto multi-task learning. In *Advances in Neural Information Processing Systems 32: Annual Conference on Neural Information Processing Systems 2019, NeurIPS 2019, 8-14 December 2019, Vancouver, BC, Canada*, pages 12037–12047, 2019. 1, 3, 4, 17

[28] Pingchuan Ma, Tao Du, and Wojciech Matusik. Efficient continuous pareto exploration in multi-task learning. In *International Conference on Machine Learning*, 2020. 1, 3, 6, 8, 17

[29] Nikhil Mishra, Mostafa Rohaninejad, Xi Chen, and Pieter Abbeel. A simple neural attentive meta-learner. In *International Conference on Learning Representations*, 2018. 7

[30] Tsendsuren Munkhdalai and Hong Yu. Meta networks. In *Proceedings of the 34th International Conference on Machine Learning, ICML 2017*, pages 2554–2563, 2017. 2, 7

[31] Boris Oreshkin, Pau Rodríguez López, and Alexandre Lacoste. Tadam: Task dependent adaptive metric for improved few-shot learning. In *Advances in Neural Information Processing Systems*, pages 721–731, 2018. 2, 7

[32] Deepak Pathak, Philipp Krahenbuhl, Jeff Donahue, Trevor Darrell, and Alexei A Efros. Context encoders: Feature learning by inpainting. In *Proceedings of the IEEE conference on computer vision and pattern recognition*, pages 2536–2544, 2016. 1, 2

[33] Siyuan Qiao, Chenxi Liu, Wei Shen, and Alan L. Yuille. Few-shot image recognition by predicting parameters from activations. In *2018 IEEE Conference on Computer Vision and Pattern Recognition, CVPR 2018, Salt Lake City, UT, USA, June 18-22, 2018*, pages 7229–7238, 2018. 7

[34] Avinash Ravichandran, Rahul Bhotika, and Stefano Soatto. Few-shot learning with embedded class models and shot-free meta training. In *2019 IEEE/CVF International Conference on Computer Vision, ICCV 2019*, pages 331–339, 2019. 7

[35] Olga Russakovsky, Jia Deng, Hao Su, Jonathan Krause, Sanjeev Satheesh, Sean Ma, Zhiheng Huang, Andrej Karpathy, Aditya Khosla, Michael Bernstein, et al. Imagenet large scale visual recognition challenge. *International journal of computer vision*, 115(3):211–252, 2015. 7

[36] Sara Sabour, Nicholas Frosst, and Geoffrey E Hinton. Dynamic routing between capsules. In *Advances in neural information processing systems*, pages 3856–3866, 2017. 7, 17

[37] Victor Garcia Satorras and Joan Bruna Estrach. Few-shot learning with graph neural networks. In *6th International Conference on Learning Representations, ICLR 2018*, 2018. 7

[38] Ozan Sener and Vladlen Koltun. Multi-task learning as multi-objective optimization. In *Advances in Neural Information Processing Systems*, pages 527–538, 2018. 2, 14

[39] Jake Snell, Kevin Swersky, and Richard S. Zemel. Prototypical networks for few-shot learning. In *Advances in Neural Information Processing Systems 30: Annual Conference on Neural Information Processing Systems 2017, 4-9 December 2017, Long Beach, CA, USA*, pages 4077–4087, 2017. 2, 7, 8

[40] Jong-Chyi Su, Subhransu Maji, and Bharath Hariharan. When does self-supervision improve few-shot learning? In *Computer Vision - ECCV 2020 - 16th European Conference, Glasgow, UK, August 23-28, 2020, Proceedings, Part VII*, pages 645–666, 2020. 1, 2, 7

[41] Flood Sung, Yongxin Yang, Li Zhang, Tao Xiang, Philip H. S. Torr, and Timothy M. Hospedales. Learning to compare: Relation network for few-shot learning. In *IEEE Conference on Computer Vision and Pattern Recognition*, pages 1199–1208, 2018. 2, 7

[42] Anupam Trivedi, Dipti Srinivasan, Krishnendu Sanyal, and Abhiroop Ghosh. A survey of multiobjec-

tive evolutionary algorithms based on decomposition. *IEEE Trans. Evol. Comput.*, 21(3):440–462, 2017. 4

[43] Kristof Van Moffaert and Ann Nowé. Multi-objective reinforcement learning using sets of pareto dominating policies. *The Journal of Machine Learning Research*, 15(1):3483–3512, 2014. 2

[44] Oriol Vinyals, Charles Blundell, Tim Lillicrap, Koray Kavukcuoglu, and Daan Wierstra. Matching networks for one shot learning. In *Advances in Neural Information Processing Systems 29: Annual Conference on Neural Information Processing Systems 2016, December 5-10, 2016, Barcelona, Spain*, pages 3630–3638, 2016. 7

[45] Teng Xiao, Shangsong Liang, and Zaiqiao Meng. Dynamic collaborative recurrent learning. In *Proceedings of the 28th ACM International Conference on Information and Knowledge Management*, pages 1151–1160, 2019. 2

[46] Teng Xiao, Shangsong Liang, Hong Shen, and Zaiqiao Meng. Neural variational hybrid collaborative filtering. *arXiv preprint arXiv:1810.05376*, 2018. 2

[47] Xu Yan, Chaoda Zheng, Zhen Li, Sheng Wang, and Shuguang Cui. Pointasnl: Robust point clouds processing using nonlocal neural networks with adaptive sampling. In *Proceedings of the IEEE/CVF Conference on Computer Vision and Pattern Recognition*, pages 5589–5598, 2020. 2

[48] Xiaohua Zhai, Avital Oliver, Alexander Kolesnikov, and Lucas Beyer. S4l: Self-supervised semi-supervised learning. In *Proceedings of the IEEE international conference on computer vision*, pages 1476–1485, 2019. 2

[49] Qingfu Zhang and Hui Li. MOEA/D: A multiobjective evolutionary algorithm based on decomposition. *IEEE Trans. Evol. Comput.*, 11(6):712–731, 2007. 4

[50] Eckart Zitzler. *Evolutionary algorithms for multiobjective optimization: methods and applications*. PhD thesis, University of Zurich, Zürich, Switzerland, 1999. 2

[51] Marcela Zuluaga, Guillaume Sergent, Andreas Krause, and Markus Püschel. Active learning for multi-objective optimization. In *International Conference on Machine Learning*, pages 462–470, 2013. 2

## A. Proofs and derivations

### A.1. Proof of Lemma

**Lemma 2:** *If  $\theta_{\pi 0}^*$  achieves the best overall performance, i.e.  $\min_{\theta} \sum_{m=1}^M L_m(\theta) = \sum_{m=1}^M L_m(\theta_{\pi 0}^*)$ , and a better performance of main task can be achieved in  $\theta'$ , i.e.,  $L_1(\theta') < L_1(\theta_{\pi 0}^*)$ , we will have  $\rho(\theta') < \rho(\theta_{\pi 0}^*)$ .*

*Proof:* We will have

$$\sum_{m=2}^M L_m(\theta') > \sum_{m=2}^M L_m(\theta_{\pi 0}^*)$$

if  $L_1(\theta') < L_1(\theta_{\pi 0}^*)$  holds.

We proof it by contradiction. If there is a  $\theta'$  satisfying

$$L_1(\theta') < L_1(\theta_{\pi 0}^*)$$

and

$$\sum_{m=2}^M L_m(\theta') < \sum_{m=2}^M L_m(\theta_{\pi 0}^*)$$

at the same time, we will have

$$\sum_{m=1}^M L_m(\theta') < \sum_{m=1}^M L_m(\theta_{\pi 0}^*) = \min_{\theta} \sum_{m=1}^M L_m(\theta).$$

However, there does not exist any  $\theta'$  satisfying

$$\sum_{m=1}^M L_m(\theta') < \min_{\theta} \sum_{m=1}^M L_m(\theta)$$

for  $\min_{\theta} \sum_{m=1}^M L_m(\theta)$  is the minimum of  $\sum_{m=1}^M L_m(\theta)$ . A contradiction is found.

Based on the above results, we have

$$\begin{aligned} \rho(\theta') &= \frac{L_1(\theta')}{\sum_{m=2}^M L_m(\theta')} \\ &< \frac{L_1(\theta_{\pi 0}^*)}{\sum_{m=2}^M L_m(\theta')} \\ &< \frac{L_1(\theta_{\pi 0}^*))}{\sum_{m=2}^M L_m(\theta_{\pi 0}^*))} \\ &= \rho(\theta_{\pi 0}^*). \end{aligned}$$

End the proof.

### A.2. Illustrating preference vectors in two-tasks scenario

Let the unit vector  $u_0$  be the direction vector of  $\rho(\theta) = \rho(\theta_0)$  in two-task scenario, let  $u_0 = (\cos \pi_0, \sin \pi_0)$ , where  $\cos \pi_0 = \frac{e_1 \mathcal{L}(\theta_{\pi 0}^*)}{\|T_2 \mathcal{L}(\theta_{\pi 0}^*)\|_2}$  and  $T_m = I - e^{mm}$ . The  $e^{mm}$  is

a single-entry matrix, i.e. the  $m$ th element in the  $m$ th column is one and the rest elements are zero,  $e_1$  is a single-entry vector, where the first element is one and rest are zero.  $I$  is an identity matrix. A set of unit preference vectors  $\{\mathbf{u}_1, \mathbf{u}_2, \dots, \mathbf{u}_K\}$ , for the preference vector  $u_i$  can be defined as:

$$\begin{aligned} u_i &= (\cos \pi_i, \sin \pi_i), \\ \text{s.t. } \pi_i &= \frac{i}{K} \left( \frac{\pi}{2} - \pi_0 \right) + \pi_0, i = 1, \dots, K. \end{aligned} \quad (12)$$

*Derivation and proof:* Instead of dividing the objective space into two parts by this hyperplane, we divide it by some vectors in two-dimensional space, for finding some special vectors in low-dimensional subspace is much easier than dividing the high-dimensional Euclidean space. We call these vectors *preference vectors* and take the three-dimensional space Oxyz as an example to illustrate our theory. If we want to divide the three-dimensional space Oxyz, we can first divide Oxyz through the vertical planes perpendicular to xOy, yOz and zOx, which are two-dimensional spaces. These vertical planes can be determined by its intersects with xOy, yOz and zOx, and the intersects can be determined by its direction vectors. Thus, dividing multi-dimensional space is equivalent to dividing multiple two-dimensional spaces, and we only need to find the direction vectors.

Considering problems in two-dimensional space is equivalent to consider problems in two-task scenario. Remind that, two-task scenario does not mean that we only have two tasks, we still have  $M$  tasks, but we pair the first task with the others, then we will have  $M-1$  pairs of tasks. We try to divide the space with these  $M-1$  pairs of tasks. Let  $u_0 = (\cos \pi_0, \sin \pi_0)$ , we obtain  $u_0$  by calculating  $\pi_0$ .

As the best overall performance can be achieved in  $\theta_{\pi_0}^*$ , we know that the hyperplane also passes  $\theta_{\pi_0}^*$ . With the solution  $\theta_{\pi_0}^*$ , we have the optimal loss vector:

$$\mathcal{L}(\theta_{\pi_0}^*) = [\mathcal{L}_1(\theta_{\pi_0}^*), \mathcal{L}_2(\theta_{\pi_0}^*), \dots, \mathcal{L}_M(\theta_{\pi_0}^*)]^T.$$

We first find the projection of the optimal loss vector, then calculate the direction vector of it as one preference vector. Take the second dimension as an example. The projection of the optimal loss vector in the second dimension is:

$$\mathcal{L}(\theta_{\pi_0}^*) = [\mathcal{L}_1(\theta_{\pi_0}^*), 0, \mathcal{L}_3(\theta_{\pi_0}^*), \dots, \mathcal{L}_M(\theta_{\pi_0}^*)]^T,$$

i.e.,  $T_2 \mathcal{L}(\theta_{\pi_0}^*)$ . Cosine of the angle between  $T_2 \mathcal{L}(\theta_{\pi_0}^*)$  and  $e_1$  is

$$\cos \pi_0 = \frac{e_1 T_2 \mathcal{L}(\theta_{\pi_0}^*)}{\|e_1\|_2 \|T_2 \mathcal{L}(\theta_{\pi_0}^*)\|_2} = \frac{e_1 \mathcal{L}(\theta_{\pi_0}^*)}{\|T_2 \mathcal{L}(\theta_{\pi_0}^*)\|_2}.$$

Remove the subspace which satisfying  $\cos \theta > \cos \pi_0$  and decompose the remaining part into  $K$  parts based on the

angles equally. As a result, we have

$$\pi_i = \frac{i}{K} \left( \frac{\pi}{2} - \pi_0 \right) + \pi_0, i = 1, \dots, K.$$

Elements in the set of vectors  $\{\mathbf{u}_1, \mathbf{u}_2, \dots, \mathbf{u}_K\}$ , i.e. preference vectors, will satisfy:

$$u_i = (\cos \pi_i, \sin \pi_i), i = 1, \dots, K.$$

Preference vectors found by this method can evenly divide the space we want. Set a proper  $K$ , we can decide the number of the divided spaces. A small  $K$  will cause the accumulation of residual error, and a big  $K$  will cost too much time and computing resources.

In our experiments, we mainly use one auxiliary task, so things are a little different. We don't need to calculate the projection of the optimal loss vector, since at this time the hyperplane is already a straight line in objective space. We straightly calculate the cosine of the angle between  $\mathcal{L}(\theta_{\pi_0}^*)$  and  $e_1$ , i.e.,

$$\cos \pi_0 = \frac{e_1 \mathcal{L}(\theta_{\pi_0}^*)}{\|e_1\|_2 \|\mathcal{L}(\theta_{\pi_0}^*)\|_2} = \frac{e_1 \mathcal{L}(\theta_{\pi_0}^*)}{\|\mathcal{L}(\theta_{\pi_0}^*)\|_2}$$

### A.3. Further discussion of preference vectors in multiple tasks

In the above section, we provide an illustration of preference vectors in two-task scenario, now we will discuss preference vectors in another perspective, with another method of finding preference vectors.

With the hyperplane  $\rho(\theta) = \rho(\theta_{\pi_0}^*)$  we can divide the objective space into two parts, and we only want the part which satisfies  $\rho(\theta) \leq \rho(\theta_{\pi_0}^*)$ . Noting that  $\rho(\theta_{\pi_0}^*)$  is a constant greater than zero, and every objective function is non-negative, the inequality

$$\rho(\theta) = \frac{L_1(\theta)}{\sum_{m=2}^M L_m(\theta)} \leq \rho(\theta_{\pi_0}^*)$$

is equivalent to

$$\frac{L_1(\theta)}{\rho(\theta_{\pi_0}^*)} \leq \sum_{m=2}^M L_m(\theta).$$

For objective function  $L_m(\theta)$ , there are two possible situations: 1)  $\frac{L_1(\theta)}{(M-1)\rho(\theta_{\pi_0}^*)} \leq L_m(\theta)$ ; 2)  $\frac{L_1(\theta)}{(M-1)\rho(\theta_{\pi_0}^*)} > L_m(\theta)$ , ( $m = 2, \dots, M$ ). We set two index sets:

$$U = \{m \mid \frac{L_1(\theta)}{(M-1)\rho(\theta_{\pi_0}^*)} \leq L_m(\theta), m \in \{2, \dots, M\}\},$$

$$V = \{m \mid \frac{L_1(\theta)}{(M-1)\rho(\theta_{\pi_0}^*)} > L_m(\theta), m \in \{2, \dots, M\}\}.$$

Clearly, we have  $U \cup V = \{2, \dots, M\}$  and  $U \cap V = \emptyset$ .  $U$  should be a non-empty subset of  $\{2, \dots, M\}$ . If  $U = \emptyset$ , we will have  $\frac{L_1(\theta)}{\rho(\theta_{\pi_0}^*)} > \sum_{m=2}^M L_m(\theta)$ , this goes against our needs.

Noting that every  $(U, V)$  can determine a partition of  $\{2, \dots, M\}$  and a subspace of the objective space, we can divide the whole space into several subspaces by setting different  $(U, V)$ . Let  $U$  run through every non-empty subset of  $\{2, \dots, M\}$  to obtain all pairs of possible  $(U, V)$ , then add  $(U, V)$  as constraints to the optimization problem. We can formulate the optimization problem as

$$\begin{aligned} \min_{\theta} \mathcal{L}(\theta) &= (\mathcal{L}_1(\theta), \mathcal{L}_2(\theta), \dots, \mathcal{L}_M(\theta))^T, \\ \text{s.t. } &\frac{L_1(\theta)}{\rho(\theta_{\pi_0}^*)} \leq \sum_{u \in U} L_u(\theta) + \sum_{v \in V} L_v(\theta), \\ &\frac{L_1(\theta)}{(M-1)\rho(\theta_{\pi_0}^*)} \leq L_m(\theta), \text{ for } m \in U, \\ &\frac{L_1(\theta)}{(M-1)\rho(\theta_{\pi_0}^*)} > L_m(\theta), \text{ for } m \in V, \\ &U \text{ is a non-empty subset of } \{2, \dots, M\}, \\ &V = \{2, \dots, M\} - U. \end{aligned} \quad (13)$$

When  $U$  running through every non-empty subset of  $\{2, \dots, M\}$ , the algorithm exploring the whole preference region.

We take the situation of  $\rho(\theta_{\pi_0}^*) = \frac{1}{M-1}$  as an example to illustrate the implication of  $(U, V)$ . If  $\rho(\theta_{\pi_0}^*) = \frac{1}{M-1}$ , then  $m \in U$  means  $L_1(\theta) \leq L_m(\theta)$ , i.e. the performance of task  $m$  is worse than the performance of main task,  $m \in V$  means  $L_1(\theta) > L_m(\theta)$ , i.e. the performance of task  $m$  is better than the performance of main task. In conclusion,  $(U, V)$  determines the relative quality between main task and auxiliary tasks, different qualities mean different subspaces. Although  $\rho(\theta_{\pi_0}^*)$  may not be equal to  $\frac{1}{M-1}$  in many situations,  $(U, V)$  can still reveal the relative quality between main task and auxiliary tasks. Thus, we can divide the objective spaces based on  $(U, V)$ .

To find the preference vectors, we only need to solve the equation group:

$$\frac{L_1(\theta)}{(M-1)\rho(\theta_{\pi_0}^*)} = L_m(\theta), m = 2, \dots, M.$$

Take the solutions of the above equation group as preference vectors, we can divide the objective space. However, we don't need to calculate the preference vectors in practice, make sure that  $U$  can run through every non-empty subset of  $\{2, \dots, M\}$  and solve the optimization problem in Eq. 13 is enough.

We can hardly decide the number of preference vectors in this method. When we just have a few tasks, preference vectors found by this method can not divide the space to too many parts, so we'd better choose the two-task scenario to divide the space. For example, when  $M = 2$ , just like our experiments,  $\{2\}$  has only one non-empty subset, and the only preference vector is the direction vector

of  $\rho(\theta) = \rho(\theta_{\pi_0}^*)$ , so we chose the two-task scenario. However, when we have plenty of tasks, it's wise to find the preference vectors in multiple tasks scenario.

#### A.4. Derivation of subproblem corresponding to the preference vectors $u_i$ and $u_{i+1}$

Given the preference vectors  $u_i$  and  $u_{i+1}$ , our next step is to add constraints to the optimization problem so that the Pareto solutions we found can lay inside between  $u_i$  and  $u_{i+1}$ . Still, we take the second dimension as an example. Firstly, we get the projection vector, then use  $\cos \pi_0 = \frac{e_1 \mathcal{L}(\theta_{\pi_0}^*)}{\|T_2 \mathcal{L}(\theta_{\pi_0}^*)\|_2}$  to measure the angle between projection vector and  $e_1$ . Let  $\cos(a, b)$  be the cosine of angle between  $a$  and  $b$ . We simply add the constraints:

$$\cos(e_1, u_i) \leq \cos(\pi_0) \leq \cos(e_1, u_{i+1})$$

to our optimization problem.  $e_1$  and  $u_i$  are both unit vectors, so  $\cos(e_1, u_i) = u_i e_1^T$ , the same as  $\cos(e_1, u_{i+1})$ . We formulate the problem as:

$$\begin{aligned} \min_{\theta} \mathcal{L}(\theta) &= (\mathcal{L}_1(\theta), \mathcal{L}_2(\theta), \dots, \mathcal{L}_M(\theta))^T, \\ \text{s.t. } &u_i e_1^T \leq \frac{e_1 \mathcal{L}(\theta)}{\|T_2 \mathcal{L}(\theta)\|_2} \leq u_{i+1} e_1^T. \end{aligned}$$

#### A.5. Rewriting the optimization problem in Eq. 8 in its dual form

The optimization problem in Eq. 8 is

$$\begin{aligned} (d_t, \alpha_t) &= \arg \min_{d \in R^M, \alpha \in R} \alpha + \frac{1}{2} \|d\|^2, \\ \text{s.t. } &\nabla \mathcal{L}_m(\theta_t)^T d \leq \alpha, i = 1, \dots, M, \\ &\nabla \mathcal{Q}_k(\theta_t)^T d \leq \alpha, k \in \mathcal{K}_\epsilon(\theta_t), \\ &\nabla \mathcal{R}_j(\theta_t)^T d \leq \alpha, j \in \mathcal{J}_\epsilon(\theta_t). \end{aligned} \quad (14)$$

It's easy to see that Eq. 8 is a convex optimization problem. To obtain the dual form of this problem, we define a Lagrangian function as

$$\begin{aligned} g(d, \alpha, \omega_m, \beta_k, \gamma_j) &= \alpha + \frac{1}{2} \|d\|^2 \\ &+ \sum_{m=1}^M \omega_m (\nabla \mathcal{L}_m(\theta_t)^T d - \alpha) \\ &+ \sum_{k \in \mathcal{K}_\epsilon(\theta_t)} \beta_k (\nabla \mathcal{Q}_k(\theta_t)^T d - \alpha) \\ &+ \sum_{j \in \mathcal{J}_\epsilon(\theta_t)} \gamma_j (\nabla \mathcal{R}_j(\theta_t)^T d - \alpha) \end{aligned}$$

Calculate the partial derivatives and solve the equation group below:

$$\begin{aligned}\frac{\partial g(d, \alpha, \omega_m, \beta_k, \gamma_j)}{\partial d} &= 0 \\ \frac{\partial g(d, \alpha, \omega_m, \beta_k, \gamma_j)}{\partial \alpha} &= 0\end{aligned}$$

These two equations are equivalent to:

$$\begin{aligned}d_t(\omega_m, \beta_k, \gamma_j) + \sum_{m=1}^M \omega_m \nabla \mathcal{L}_m(\theta_t) \\ + \sum_{k \in \mathcal{K}_\epsilon(\theta_t)} \beta_k \nabla \mathcal{Q}_k(\theta_t) \\ + \sum_{j \in \mathcal{J}_\epsilon(\theta_t)} \gamma_j \nabla \mathcal{R}_j(\theta_t) &= 0\end{aligned}$$

and

$$1 - \left( \sum_{i=1}^M \omega_m + \sum_{k \in \mathcal{K}_\epsilon(\theta_t)} \beta_k + \sum_{j \in \mathcal{J}_\epsilon(\theta_t)} \gamma_j \right) = 0.$$

It's easy to see that  $d_t(\omega_m, \beta_k, \gamma_j)$  is a function of every  $\omega_m, \beta_k$ , and  $\gamma_j$ . We replace the  $d$  in Eq. 8 with  $d_t(\omega_m, \beta_k, \gamma_j)$ , and add the constraint  $\sum_{i=1}^M \omega_m + \sum_{k \in \mathcal{K}_\epsilon(\theta_t)} \beta_k + \sum_{j \in \mathcal{J}_\epsilon(\theta_t)} \gamma_j = 1$  to the optimization problem so that we could omit  $\alpha$  in Eq. 8. In the end, we formulate the optimization problem as

$$\begin{aligned}\max_{\omega_m, \beta_k, \gamma_j} & -\frac{1}{2} \|d_t(\omega_m, \beta_k, \gamma_j)\|_2^2, \\ \text{s.t. } & \sum_{i=1}^M \omega_m + \sum_{k \in \mathcal{K}_\epsilon(\theta_t)} \beta_k + \sum_{j \in \mathcal{J}_\epsilon(\theta_t)} \gamma_j = 1, \\ & \forall m = 1, \dots, M, \forall k \in \mathcal{K}_\epsilon(\theta_t), \forall j \in \mathcal{J}_\epsilon(\theta_t), \\ & \omega_m \geq 0, \beta_k \geq 0, \gamma_j \geq 0.\end{aligned}\tag{15}$$

## A.6. Finding the update direction in Pareto exploration

Assuming that Pareto front is so smooth that every point on this front can be passed through by several smooth curves on this front. Let  $\theta^*$  be a Pareto solution and  $\theta_{(x)} : (-\epsilon, \epsilon) \rightarrow \mathbb{R}^n$  is a smooth curve on Pareto front which pass through  $\theta^*$  in 0, i.e.,  $\theta_{(0)} = \theta^*$ . Our aim is to find some other Pareto optimal solutions, i.e., find some other points on the Pareto front. Finding points on the Pareto front directly is too costly, so we first try to find some approximations of Pareto solutions, then optimize these approximations to find the exact Pareto solutions.

We need to calculate the first-order approximation, i.e., calculate  $\theta_1 = \theta_{(0)} + \eta \frac{d\theta}{dx}(0)$ . As mentioned in Lemma 3,

for every Pareto solution, we have

$$\sum_{m=1}^M \lambda_m \nabla \mathcal{L}_m(\theta^*) = \mathbf{0},$$

where  $\lambda \in \mathbb{R}^M$ ,  $\lambda_m \geq 0$ ,  $\sum_{m=1}^M \lambda_m = 1$ . Thus, for every point on the curve  $\theta_{(x)}$ , we have

$$\sum_{m=1}^M \lambda_m(\theta_{(x)}) \nabla \mathcal{L}_m(\theta_{(x)}) = \mathbf{0}.$$

$\lambda_m$  will change if  $\theta_{(x)}$  changes, so we write  $\lambda_m$  as a function of  $\theta_{(x)}$ , i.e.  $\lambda_m(\theta_{(x)})$ . Differentiate both sides of the equation, we will have

$$\mathbf{H}(\theta^*) \frac{d\theta}{dx}(0) = \nabla \mathcal{L}(\theta^*)^\top \beta,$$

where  $\mathbf{H}(\theta^*) = \sum_{m=1}^M \lambda_m \nabla^2 \mathcal{L}_m(\theta^*)$  and  $\beta \in \mathbb{R}^M$ . We can obtain  $\frac{d\theta}{dx}(0)$  by this method.

However, solving a large-scale linear equation group is very costly in practice. As suggested by Sener and Koltun[38], we get  $\lambda$  by solving a convex optimization problem below:

$$\begin{aligned}\min_{\lambda} & \left\| \sum_{m=1}^M \lambda_m \nabla \mathcal{L}_m(\theta_{(x)}) \right\|_2 \\ \text{s.t. } & \lambda \geq \mathbf{0}, \quad \sum_{m=1}^M \lambda_m = 1\end{aligned}$$

Get  $\lambda$  for  $\nabla \mathcal{L}(\theta_{(x)})$  and calculate  $\frac{d\theta}{dx}(0)$ , then we will be able to have the approximation  $\theta_1$ . Optimize  $\theta_1$ , we can have another Pareto solution.

Notation	Description
$I_d, J_d, L_d$	No. of users, items and criteria
$\mathbf{R}_d = [r_{d,ijl}]_{I_d \times J_d \times L_d}$	User-item-criterion ratings
$\mathbf{U}_d, \mathbf{V}_d, \mathbf{C}_d$	Latent factor matrix
$\mathcal{G}$	Core tensor of Tucker
$\mathbf{u}_{d,i}, 1 \leq i \leq I_d$	Latent factor vector of users
$I_d, J_d, L_d$	No. of users, items and criteria
$\mathbf{R}_d = [r_{d,ijl}]_{I_d \times J_d \times L_d}$	User-item-criterion ratings
$\mathbf{U}_d, \mathbf{V}_d, \mathbf{C}_d$	Latent factor matrix
$\mathcal{G}$	Core tensor of Tucker
$\mathbf{u}_{d,i}, 1 \leq i \leq I_d$	Latent factor vector of users

Table 5: Summary of primary notations.

## B. Additional implementation details

### B.1. Network architectures

**Conv-4-64.** It consists of 4 convolutional blocks each implemented with a  $3 \times 3$  convolutional layer with 64 channels followed by BatchNorm + ReLU +  $2 \times 2$  max-pooling

units. In the MiniImageNet experiments for which the image size is  $84 \times 84$  pixels, its output feature map has size  $5 \times 5 \times 64$  and is flattened into a final 1600-dimensional feature vector. For the CIFAR-FS experiments, the image size is  $32 \times 32$  pixels, the output feature map has size  $2 \times 2 \times 64$  and is flattened into a 256-dimensional feature vector

**WRN-28-10.** It is a Wide Residual Network with 28 convolutional layers and width factor 10. The 12 residual layers of this architecture are grouped into 3 residual blocks (4 residual layers per block). In the MiniImageNet experiments, the network gets as input images of size  $80 \times 80$  (rescaled from  $84 \times 84$ ), and during feature extraction each residual block downsamples by a factor of 2 the processed feature maps. Therefore, the output feature map has size  $10 \times 10 \times 640$  which, after global average pooling, creates a 640-dimensional feature vector. In the CIFAR-FS experiments, the input images have size  $32 \times 32$  and during feature extraction only the last two residual blocks downsample the processed feature maps. Therefore, in the CIFAR-FS experiments, the output feature map has size  $8 \times 8 \times 640$  which again after global average pooling creates a 640-dimensional feature vector.

**Rotation prediction network.** This network gets as input the output feature maps of  $\theta_1$  and is implemented as a convnet. More specifically, for the Conv-4-64 and Conv-4-512 feature extractor architectures (regardless of the dataset), The network consists of two  $3 \times 3$  convolutional layers with BatchNorm + ReLU units, followed by a fully connected classification layer. For Conv-4-64, those two convolutional layers have 128 and 256 feature channels respectively, while for Conv-4-512 both convolutional layers have 512 feature channels. In the WRN-28-10 case, The network consists of a 4-residual-layer residual block that actually replicates the last (3rd) residual block of WRN-28-10. This residual block is followed by global average pooling plus a fully connected classification layer.

**Relative patch location network.** Given two patches, The network gets the concatenation of their feature vectors extracted with  $\theta_1$  as input, and forwards it to two fully connected layers. The single hidden layer, which includes BatchNorm + ReLU units, has 256, 1024, and 1280 channels for the Conv-4-64, Conv-4-512, and WRN-28-10 architectures respectively.

## B.2. Incorporating self-supervision during training

Here we provide more implementation details regarding how we incorporate self-supervision during the training stage.

**Training with rotation prediction self-supervision.** During training for each image of a mini-batch we create its 4 rotated copies and apply to them the rotation prediction task (i.e.,  $L_2$  loss). When training the object classifier with rotation augmentation (e.g., CC-based models) the ob-

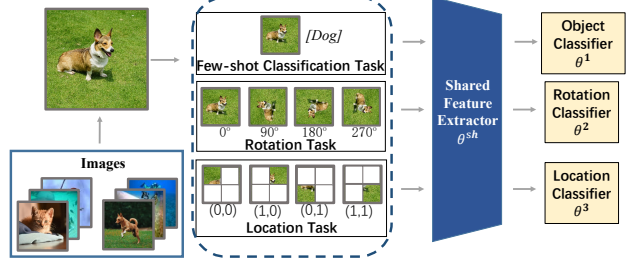


Figure 8: The framework used in our Pareto Self-Supervised Training.

ject classification task (i.e.,  $L_1$  loss) is applied to all rotated versions of the images. Otherwise, only the upright images (i.e., the 0 degrees images) are used for the object classification task. Note that in the PN-based models, we apply the rotation task to both the support and the query images of a training episode, and also we do not use rotation augmentation for the object classification task.

**Training with relative patch location self-supervision.** In this case during training each mini-batch includes two types of visual data, images and patches. Similar to [16], in order to create patches, an image is: (1) resized to  $96 \times 96$  pixels (from  $84 \times 84$ ), (2) converted to grayscale with probability 0.66, and then (3) divided into 9 regions of size  $32 \times 32$  with a  $3 \times 3$  regular grid. From each  $32 \times 32$  sized region we (4) randomly sample a  $24 \times 24$  patch, and then (5) normalize the pixels of the patch individually to have zero mean and unit standard deviation. The object classification task is applied to the image data of the mini-batch while the relative patch location task to the patch data of the mini-batch. Also, as already explained, we also apply an extra auxiliary object classification loss to the patch data.

## B.3. Training routine for training stage

To optimize the training loss we use mini-batch SGD optimizer with momentum 0.9 and weight decay  $5e-4$ . In the MiniImageNet and CIFAR-FS experiments, we train the models for 60 epochs (each with 1000 SGD iterations), starting with a learning rate of 0.1 which is decreased by a factor of 10 every 20 epochs. The mini-batch sizes were cross-validated on the validation split. For instance, the models based on CC and Conv-4-64, Conv-4-512, or WRN-28-10 architectures are trained with mini-batch sizes equal to 128, 128, or 64 respectively. Finally, we perform early stopping w.r.t. the few-shot classification accuracy on the validation novel classes (for the CC-based models we use the 1-shot classification accuracy).

## C. More details of Few-Shot Auxiliary Learning

The main component of all few-shot algorithms is a feature extractor  $\theta^{sh}$ . As shown in Fig. 8, given an image  $x$ , the feature extractor will output a  $d$ -dimensional feature  $\theta^{sh}(x)$  to different classifier, and the object classifier  $\theta^1$  will output the label of image. In this work, we use Cosine Classifiers (CC) [17] as object classifier.

**Cosine Classifiers.** In CC few-shot learning, the first stage trains the feature extractor  $\theta^{sh}$  together with a cosine-similarity based classifier on the (standard) supervised task of classifying the base classes. Denoting  $\theta_1 = [\mathbf{w}_1, \dots, \mathbf{w}_{N_b}]$  the matrix of the  $d$ -dimensional classification weight vectors, the normalized score for an input image  $\mathbf{x}$  is

$$C^j(\theta^{sh}(\mathbf{x}); \theta_1) = \text{softmax}_j \left[ \gamma \cos(\theta^{sh}(\mathbf{x}), \mathbf{w}_i)_{i \in Y_b} \right] \quad (16)$$

where  $\cos(\cdot, \cdot)$  is the cosine operation between two vectors, and the scalar  $\gamma$  is the inverse temperature parameter of the softmax operator,  $j$  is the class. The training stage aims at minimizing w.r.t.  $\theta^{sh}$  and  $\theta_1$  the negative log-likelihood loss:

$$\mathcal{L}_1(\theta^{sh}, \theta_1; D_b) = \mathbb{E}_{(\mathbf{x}, y) \sim D_b} [-\log C^y(\theta^{sh}(\mathbf{x}); \theta_1)] \quad (17)$$

One of the reasons for using the cosine-similarity based classifier instead of the standard dot-product based one, is that the former learns feature extractors that reduce intra-class variations and thus can generalize better on novel classes. The weight vectors  $w_j$  in  $\theta_1$  can be interpreted as learned prototypes for the base classes, to which input image features are compared for classification. The second stage boils down to computing one representative feature  $w_j$  for each new class by simple averaging of associated  $K$  samples in  $D_n$ , and to define the final classifier  $C(\cdot; [\mathbf{w}_1 \dots \mathbf{w}_{N_n}])$ .

**Self-Supervised Auxiliary loss** We incorporate self-supervision to a few-shot learning algorithm by adding an auxiliary self-supervised loss during its training stage. More formally, let  $\mathcal{L}_2(\theta^{sh}, \theta^2; X_b)$  be the self-supervised loss applied to the set  $X_b = \{\mathbf{x} \mid (\mathbf{x}, y) \in D_b\}$  of training examples in  $D_b$  deprived of their class labels. The loss  $\mathcal{L}_2(\theta^{sh}, \theta^2; X_b)$  is a function of the parameters  $\theta^{sh}$  of the feature extractor and of the parameters  $\theta^2$  of a network only dedicated to the self-supervised task. The first training stage of few-shot auxiliary learning is

$$\min_{\theta^{sh}, \theta^1, \theta^2} \omega_1 \mathcal{L}_1(\theta^{sh}, \theta^1; D_b) + \omega_2 \mathcal{L}_2(\theta^{sh}, \theta^2; X_b) \quad (18)$$

where the positive hyperparameter  $\omega_1$  and  $\omega_2$  controls the importance of the classification term and self-supervised

term. The framework of the approach is provided in Figure 8. For the self-supervised loss, we consider two-task in the present work: predicting the rotation incurred by an image [18], which is simple and readily incorporated into a few-shot learning algorithm; predicting the relative location of two patches from the same image [9], a seminal task in self-supervised learning. In a recent study, both methods have been shown to achieve state-of-the-art results [24].

**Image rotations.** In this task, the convnet must recognize among four possible 2D rotations in  $\mathcal{R} = \{0^\circ, 90^\circ, 180^\circ, 270^\circ\}$  the one applied to an image (see Figure 8). Specifically, given an image  $x$ , we first create its four rotated copies  $\{\mathbf{x}^r \mid r \in \mathcal{R}\}$ , where  $x^r$  is the image  $x$  rotated by  $r$  degrees. Based on the features  $\theta^{sh}(\mathbf{x}^r)$  extracted from such a rotated image, the new network  $\theta^2$  attempts to predict the rotation class  $r$ . Accordingly, the self-supervised loss

$$\mathcal{L}_2(\theta^{sh}, \theta^2; X) = \mathbb{E}_{\mathbf{x} \sim X} \left[ \sum_{\forall r \in \mathcal{R}} -\log \theta^2(\theta^{sh}(\mathbf{x}^r)) \right] \quad (19)$$

where  $X$  is the original training set of non-rotated images and  $\theta^2(\cdot)$  is the predicted normalized score for rotation  $r$ . Intuitively, in order to do well for this task the model should reduce the bias towards up-right oriented images, typical for ImageNet-like datasets, and learn more diverse features to disentangle classes in the low-data regime.

**Relative patch location.** Here, we create random pairs of patches from an image and then predict, among eight possible positions, the location of the second patch w.r.t. to the first, e.g., “on the left and above” or “on the right and below”. Specifically, given an image  $x$ , we first divide it into 9 regions over a  $3 \times 3$  grid and sample a patch within each region. Let’s denote  $x^0$  the central image patch, and  $x^1 \dots x^8$  its eight neighbors lexicographically ordered. We compute the representation of each patch and then generate patch feature pairs  $(\theta^{sh}(x^0), \theta^{sh}(x^p))$  by concatenation. We train a fully-connected network  $\theta^3(\cdot, \cdot)$  to predict the position of  $x^p$  from each pair. The self-supervised loss of this task is defined as:

$$\mathcal{L}_3(\theta^{sh}, \theta^3; X) = \mathbb{E}_{\mathbf{x} \sim X} \left[ \sum_{p=1}^8 -\log \theta^3(\theta^{sh}(x^0), \theta^{sh}(x^p)) \right] \quad (20)$$

where  $X$  is a set of images and  $\theta^3$  is the predicted normalized score for the relative location  $p$ .

## D. More details of Pareto exploration

### D.1. MultiMNIST Setup

We first generated the full MultiMNIST dataset and picked a subset of 2048 images, downsampled from  $28 \times 28$  to  $14 \times 14$ , as our MultiMNIST Subset example. The

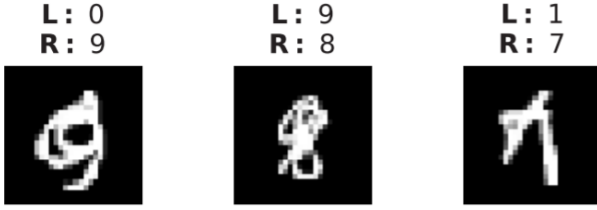


Figure 9: Sample images from MultiMNIST. Above each image are the labels of the upper-left (L) and lower-right (R) items.

two objectives are the cross entropy losses of classifying the top-left and bottom-right digits evaluated on all 2048 images. Regarding the classifier, we used a modified network, which has 1500 parameters. Our modified network starts with a convolutional layer with 10 channels, a  $5 \times 5$  kernel, and a stride of 2 pixels, followed by a  $2 \times 2$  max pooling layer. Next, the results are fed into a fully connected layer of size  $20 \times 10$  and then sent to two fully connected layers, one for each task. We use ReLU as the non-linear function in the network. Essentially, this synthetic example attempts to use a small network to overfit 2048 images. To generate the Pareto front, we ran BFGS to optimize  $w_1 f_1 + w_2 f_2$  with  $w_1 = 0, 0.01, 0.02, \dots, 1$  from the same random initial guess, which generated a list of 101 solutions  $\mathbf{x}_0^*, \mathbf{x}_1^*, \mathbf{x}_2^*, \dots, \mathbf{x}_{101}^*$ . We then linearly interpolated  $\mathbf{f}(\mathbf{x}_i^*)$ ,  $i = 0, 1, 2, \dots, 100$  and treat the resulting piecewise linear spline as the (empirical) Pareto front.

**Dataset and Task Description.** We followed [36] to generate MultiMNIST. We first created  $36 \times 36$  images by placing two  $28 \times 28$  images from MNIST in the upper-left and lower-right corner with a random shift of up to 2 pixels in each direction. The synthesized images were then resized to  $28 \times 28$  and normalized with a mean of 0.1307 and a standard deviation of 0.3081. No data augmentation was used for training or testing. Following [27, 28], we built MultiMNIST from MNIST as shown in the Figure 9. Each dataset has 60,000 training images and 10,000 test images. The objectives are the cross entropy losses of classifying the upper-left and lower right items in the image.

**Network Architecture.** The backbone network is a modified LeNet (LeCun et al., 1998). Our network starts from two convolutional layers with a  $5 \times 5$  kernel and a stride of 1 pixel. The two layers have 10 and 20 channels respectively. A fully connected layer of 50 channels appends the convolutional layers, which is then followed by two 10-channel fully connected layers, one for each task. We add a  $2 \times 2$  max pooling layer right after each convolutional layer and use ReLU as the nonlinear function. The network contains 22,350 trainable parameters.

**Training** Training We trained all baselines for 30 epochs

of SGD. We used 256 as our mini-batch size and set the momentum to 0.9. The learning rate started from 0.01 and decayed with a cosine annealing scheduler.

## D.2. Details of exploration on the tangent plane.

**Find gradient on the tangent plane at  $\theta^*$ .** Once a Pareto solution  $\theta^*$  is found, we explore its local Pareto set by spawning new points  $\theta_t$ .

**Lemma 3** [23]: If  $\theta^*$  is Pareto optimal, there will be a  $\lambda \in \mathbb{R}^M$  such that  $\lambda_m \geq 0$ ,  $\sum_{m=1}^M \lambda_i = 1$ , and  $\sum_{m=1}^M \lambda_m \nabla \mathcal{L}_m(\theta^*) = \mathbf{0}$ .

**Proposition** [22]: Assuming that  $\mathcal{L}(\theta^*)$  is smooth and  $\theta^*$  is Pareto optimal, consider any smooth curve  $\theta_{(x)} : (-\epsilon, \epsilon) \rightarrow \mathbb{R}^n$  in the Pareto set and passing  $\theta^*$  at  $x = 0$ , i.e.,  $\theta_{(0)} = \theta^*$ , then  $\exists \beta \in \mathbb{R}^M$  such that:

$$\mathbf{H}(\theta^*) \frac{d\theta}{dx}(0) = \nabla \mathcal{L}(\theta^*)^\top \beta \quad (21)$$

where  $\mathbf{H}(\theta^*) = \sum_{m=1}^M \lambda_i \nabla^2 \mathcal{L}_m(\theta^*)$ .

We use  $\frac{d\theta}{dx}(0)$  as the update direction and calculate  $\theta_1 = \theta_{(0)} + \eta \frac{d\theta}{dx}(0)$ .

Solving such problem requires an efficient matrix solver. Similar to [28], we use Krylov subspace iteration methods, because they are matrix-free and iterative solvers, allowing us to solve the system without complete Hessians and terminate with intermediate results. In our experiment, we choose to use the minimal residual method (MINRES), a classic Krylov subspace method designed for symmetric indefinite matrices. Note that early termination in MINRES still returns meaningful results because the residual error is guaranteed to decrease monotonically with iterations. To summarize, the efficiency of our exploration algorithm comes from two sources: exploration on the tangent plane and early termination from a matrix-free, iterative solver. The time cost of getting one tangent direction is  $O(kn)$ , which scales linearly to the network size.